4、 外语能力证书

中国科学院武汉科技查新咨询检索中心

检 索 报 告

（报告编号：2025-WJ-0909-3）

委托单位：红河学院

委 托 人：石玲

检索要求：2021 年发表第一作者论文 “One-step Synthesis of Ultrasmall Platinum Nanoparticles Supported on Amino-Functionalized Graphene to Create an Electrochemical Molecularly Imprinted Polymer Sensor for Fluxapyroxad”被 SCIE 收录与相关期刊 2021 年升级版分区情况

检 索 结 果

数据库	论文收录(篇)
SCIENCE CITATION INDEX-EXPANDED	1

数据库	2021 年文献分区情况			
中国科学院文献情报中心期刊分区表-升级版	分区	1 区	2 区	3 区	4 区
	篇数	0	0	0	1

*相关期刊分区信息见附件。

声明	委托人须要求说明，视为已对本法明所列内关键其核对，确认无误，若有不实，概由委托人承担全部责任。
检索人	万杰	审核人	余

中国科学院文献情报中心检索中心

2025.09.09

联系人：万杰 手机/电话：027-87197719

邮箱：chinalis@mail.las.ac.cn

主页：www.chinalis.las.ac.cn

地址：武汉市武昌区中南路 25 号

中国科学院武汉科技查新咨询检索中心

检索附件：SCIE 收录论文及相关期刊 2021 年升级版分区情况

Record 1 of 1
Title: One-step Synthesis of Ultrasmall Platinum Nanoparticles Supported on Amino-Functionalized Graphene to Create an Electrochemical Molecularly Imprinted Polymer Sensor for Fluxapyroxad
Author(s): Liu, Ling; Duan, Jie; Duan, Jidong; Dan, Jiaqi; Xu, Shufang; Yang, HP (Yang, Hongping); Yang, GM (Yang, Guangming)
Source: INTERNATIONAL JOURNAL OF ELECTROCHEMICAL SCIENCE Volume: 16 Issue: 7 Article Number: 210767 DOI: 10.20964/2021.07.19 Published Date: 2021 JUL
Times Cited in Web of Science Core Collection: 3
Total Times Cited: 3
Accession Number: WOS:000669332100065
Language: English
Document Type: Article
Addresses: [Liu, Ling; Duan, Jie; Xu, Shufang; Yang, Guangming] Honghe Univ, Coll Sci, Engn Res Ctr Proc & Qual Control Local Characteristic Food & Cosmet Goods, Mengzi 661199, Yunnan, Peoples R China
[Yang, Hongping] Honghe Univ, Mengzi 661199, Yunnan, Peoples R China
Corresponding Address: Yang, GM (corresponding author), Honghe Univ, Coll Sci, Engn Res Ctr Proc & Qual Control Local Characteristic Food & Cosmet Goods, Mengzi 661199, Peoples R China.
E-mail Addresses: yangguangming@126.com
Categories/Classification: Science Citation Index Expanded (SCI-EXPANDED)
Web of Science Index: ESCI
ISSN: 1452-3981
期刊 2021 年中国科学院文献情报中心升级版分区情况
刊名 International Journal of Electrochemical Science
年份 2021
ISSN 1452-3981
Review 否
Open Access 否
Web of Science SCIE

学科	分区 Top 期刊
大类 化学	4 区
小类 ELECTROCHEMISTRY 电化学	4 区

(END)

Int. J. Electrochem. Sci., 16 (2021) Article ID: 210767, doi: 10.20964/2021.07.19

International Journal of ELECTROCHEMICAL SCIENCE
www.electrochemsci.org

One-step Synthesis of Ultrasmall Platinum Nanoparticles Supported on Amino-Functionalized Graphene to Create an Electrochemical Molecularly Imprinted Polymer Sensor for Fluxapyroxad

Ling Shi[1], Jie Duan[1], Shufang Xu[1], Hongping Yang[2], Guangming Yang[1,]*

[1] Engineering Research Center for Processing and Quality Control of Local Characteristic Food and Cosmetic Goods of High Education in Yunnan Province, College of Science, Honghe University, Mengzi 661199, PR China
[2] Library, Honghe University, Mengzi 661199, PR China
[*]E-mail: yangguangming@126.com

Received: 22 February 2021 / *Accepted:* 15 April 2021 / *Published:* 31 May 2021

In this work, a novel electrochemical molecularly imprinted polymer (MIP) sensor for fluxapyroxad (FP) was constructed. This MIP sensor was based on indole-6-carboxylic acid (6-IAA) and platinum (Pt) nanoparticles (NPs) supported amino-functionalized graphene (NH$_2$-rGO). Massive and ultrasmall Pt NPs (2-3 nm) were supported on NH$_2$-rGO, which was easily prepared using a simple, aqueous phase method. Pt NP was firstly generated using ascorbic acid as the reducant and hexadecylpyridinium chloride as the structure-directing agent; then, NPs were immediately loaded on the surface of NH$_2$-rGO to create Pt-NPs-NH$_2$-rGO. Later, the MIP film was formed by electropolymerizing Pt-NPs-NH$_2$-rGO/6-IAA mixture solution. This hybrid material was then used to modify the glassy carbon electrode (GCE) surface, resulting in a Pt-NPs-NH$_2$-rGO / GCE. After this modifications, FP was imprinted on the aforementioned electrode surface using cyclic voltammetry, with 6-IAA as the functional monomer. Finally, FP was eluted from the polymer, resulting in the MIP sensor. After rebinding the template molecules Fe(CN)$_6^{3-/4-}$ was used to measure the impedance of the MIP sensor. Results indicated an excellent response for FP across a linear range of 1.0 × 10^{-10} to 1.3 × 10^{-5} mol L^{-1}; the detection limit was determined to be 1.0 × 10^{-10} mol L^{-1} (S/N= 3). This sensor was also used to detect FP in real samples, with results indicating it was a reliable sensor for FP.

Keywords: Electrochemical sensor; Fluxapyroxad; Molecularly imprinted polymer; Indole-6-carboxylic acid; Pt nanoparticles; Amino group functionalized-graphene

1. INTRODUCTION

Fluxapyroxad (FP) belongs to pyrazole fungicides, which is a new group of pesticides that are widely used to control fungal diseases in agricultural products [1]. Notably, FP has an inherently high

chemical stability, resulting in extensive residues after its use both on food and in the environment. Critically, these residues cause a variety of unpredictable risks to human health [2, 3]. Based on these potential health effects, many countries have set a maximum residue limit for FP in their food-safety control programs [3, 4]. Given this, it has become necessary to construct a sensitive and effective analytical method for monitoring FP residues in food products.

Currently, gas chromatography-tandem mass spectrometry (GC-MS / MS) [4] and liquid chromatography-tandem mass spectrometry (LC-MS / MS) [5, 6] have all been used to determine FP residues in food samples. These techniques have been used owing to their high precision and sensitivity; however, these methods usually involve tedious protocols and high costs. Thus, an electrochemical method would offer an alternative approach, owing to its advantageous simplicity, low cost, and high sensitivity when compared with traditional methods (e.g., GC-MS / MS and LC-MS / MS) [7-9]. Despite this potential, there remains no published work on the application of electrochemical methods to determine FP residues.

Electrochemical molecularly imprinted polymer (MIP) sensors have become a popular tool for the detection of pesticides. The performance of MIP sensors, including their respective sensitivities and selectivities, are closely related to the exposure of the imprinted sites on the sensing interface [7, 10]. Given this, using a surface imprinting is a promising strategy to improve the total amount of imprinted sites [11, 12]. Electrochemical polymerization has been widely used to prepare MIPs on an electrode surface. This approach has also been viewed as an ideal surface imprinting method, since it is simple, controllable, and highly efficient [12]. Moreover, conductive nanomaterials that have large, specific surface areas, such as graphene (r-GO), carbon nanotubes, metal nanomaterials, and their hybrid composites, would provide a large surface area for imprinting polymerization and allow for fast mass transfer [10, 11]. At the same time, the structure of the polymer is also an important factor for their performance. Regarding these polymers, polyaniline, polypyrrole, polythiophene, and their derivatives typically have tight structures, which reduce mass transfer and specific recognition sites [12]. Recently, we reported a MIP sensor for florfenicol based on poly-indole-3-carboxylic acid, which presented with a three-dimensional, porous structure [13]. Given these preliminary findings, further work is needed regarding the utility of a porous polymer for MIP-based sensors.

The hybrid nanocomposites of graphene (r-GO) and metal nanoparticles (NPs) have attracted a strong scientific interest for their use in electrochemical MIP sensors. This interest has been driven largely by their intrinsic physical properties, such as their high electrical conductivities, large surface areas, and excellent electrochemical performance as well as their chemical characteristics (e.g., modifiable surface and functional groups) [14-16]. Given this and to improve its properties, r-GO has been typically used as a supporter to load NPs. There are two main strategies to form these composites: (1) Mixing as-prepared materials and (2) using an *in situ* preparation method. In generally, the latter offers more advantages, including a fast, efficient, and easy process. However, the supported amount of NPs on the r-GO surface have typically been insufficient, with correspondingly large diameters [14, 16, 17]. As a result, this approach has remained challenging.

In this work, Pt NPs with a small diameter (2-3 nm) were prepared using hexadecylpyridinium chloride (HDPC) as the structure-directing agent. These Pt NPs were then loaded *in situ* on the surface of NH$_2$-r-GO to form a hybrid, nanocomposite of Pt-NPs-NH$_2$-r-GO that featured an interreaction

between the amino group and Pt. After, the hybrid material was used to modified electrode. FP was imprinted on above modified surface using cyclic voltammetry (CV), with indole-6-carboxylic acid (6-IAA) as the functional monomer and FP as the template molecule. Using this approach, a MIP electrochemical sensor for FP was successfully achieved. For this strategy, the massive, ultrasmall Pt NPs were easily supported on the NH$_2$-r-GO surface using a one-step synthesis. To our knowledge, this is the first time 6-IAA has been used as a monomer for MIP; it is also the first time an electrochemical MIP sensor for FP has been constructed.

2. MATERIALS AND METHODS

2.1 Chemicals

NH$_2$-graphene (NH$_2$-r-GO) was obtained from Nanjing XFNANO Materials Tech Co., Ltd. (Nanjing, China). Hexadecylpyridinium chloride monohydrate ($C_5H_5N(CH_2)_{15}CH_3$·H_2O, HDPC, 99.0%), Chloroplatinic acid (H_2PtCl_6), indole-6-carboxylic acid (6-IAA, 99.0%), fluxapyroxad (99.9%), ascorbic acid ($C_6H_8O_6$, AA, 99.0%), fenofen (99.9%), and pyraclostrobin (99.9%) were all obtained from J&K Scientific Ltd. (Beijing, China). The phosphate buffer solution (PBS, pH=5.8) was prepared with Na_2HPO_4 and NaH_2PO_4, and this buffer was used to dissolve FP to prepare a FP stock solution. Purified water (18 MΩ cm^{-1}) was used in all experiments.

2.2 Synthesis of Pt-NPs-NH$_2$-r-GO

Briefly, 40 mg HDPC was dispersed in 10 mL NH$_2$-r-GO suspension (1.0 mg mL^{-1}). Then, 0.8 mL of 10 mmol L^{-1} H_2PtCl_6 was added into above solution to obtain a homogeneous dispersion. In succession, 6.60 mL of AA (0.10 mol L^{-1}) was added into above dispersion, and kept undisturbed at 90°C for 3 h. The products were harvested via centrifugation and washed three times with H_2O and ethanol, respectively. Finally, the product was redispersed with H_2O, yielding a 1 mg mL^{-1} Pt-NPs-NH$_2$-r-GO suspension.

2.4. Preparation of the MIP electrochemical sensor

The preparation of the MIP sensor is shown in Scheme 1. First, 5 μL 1 mg mL^{-1} of Pt-NPs-NH$_2$-r-GO suspension was dropped onto the clean GCE surface, after which it was dried under an infrared lamp to obtain Pt-NPs-NH$_2$-r-GO / GCE. Then, Pt-NPs-NH$_2$-r-GO / GCE was immersed in an acetonitrile solution containing template molecule (FP, 0.1 mmol L^{-1}), functional monomer (6-IAA, 0.4 mmol L^{-1}), and electrolyte (tetrabutylammonium perchlorate, 0.1 mol L^{-1}). Afterwards, CV measurements were performed with Pt NPs-NH$_2$-r-GO / GCE as working electrode using a scan rate of 50 mV s^{-1} and a potential range of 0 to 1.3 V. After 16 cycles, the resulting electrode was immersed in a methanol / acetic acid (9 / 1, V / V) solution for 20 min to elute the template molecule. After immersion, the final MIP / Pt NPs-NH$_2$-r-GO / GCE was produced. The non-imprinted polymer (NIP)

sensor was prepared using the same preparation conditions as the MIP sensor, with exception that no template was used. MIP-NH$_2$-r-GO / GCE was also fabricated identical to MIP / Pt NPs-NH$_2$-r-GO / GCE, but its polymerized substrate was NH$_2$-r-GO / GCE.

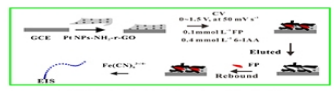

Scheme 1. The Scheme for the construction of MIP sensor.

2.5. Electrochemical measurements

MIP / Pt NPs-NH$_2$-r-GO / GCE was immersed in a 10 mL FP aqueous solution (pH=5.8) under mild magnetic stirring to allow recognition of the template molecules. After 400 s, the MIP / Pt NPs-NH$_2$-r-GO / GCE was rinsed with H_2O and immersed in a Fe(CN)$_6^{3-/4-}$ aqueous solution containing 2.5 mmol L^{-1} $K_4Fe(CN)_6$, 2.5 mmol L^{-1} $K_3Fe(CN)_6$, and 0.1 mol L^{-1} KCl. This was then used as the working electrode in subsequent electrochemical impedance spectroscopy (EIS) measurements.

3. RESULTS AND DISCUSSION

3.1 Morphology and structure of Pt NPs-NH$_2$-r-GO

Firstly, transmission electron microscopy (TEM) was used to record the morphological structure of the as-prepared products. TEM images of NH$_2$-r-GO indicated a characteristic wrinkled structure and either single or thinly layered sheets (Figure 1A). Results indicated that a large amount of Pt NPs were loaded on its surface (Figure 1B); the diameters of Pt NPs were 2-3 nm (Figure 1C). As previously described, Pt NPs were first synthesized under the structure-directing effect of HDPC; then, the NPs were immediately loaded onto the NH$_2$-r-GO surface. This loading occured because of the interaction between the amino group and Pt. This is different from our previous report, which showed the formation of a three-dimensional, porous Pt fame structure [18]. In this previous work, the structure formed in the absence of NH$_2$-r-GO in the reaction solution and was attributed to an

interreaction that was stronger than the directing effect of HDPC in the formation of the frame structure.

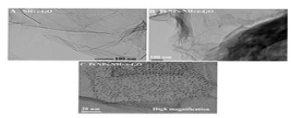

Figure 1. TEM images of NH$_2$-r-GO (A) and Pt NPs-NH$_2$-r-GO (B-C).

Next, scanning electron microscope (SEM) images of Pt NPs-NH$_2$-r-GO / GCE also indicated a characteristic wrinkled structure, which was in accordance with its TEM images. When MIP was successfully prepared on Pt NPs-NH$_2$-r-GO / GC (Figure 2A), its SEM image indicated porous, three-dimensional networks (Figure 2B). These network diameters were approximately 100 nm and were visually apparent even at low magnification image (Figure S1). Importantly, this finding was notably different from our previous report, which used 5-IAA as a functional monomer (Figure S2) [13]. This difference is attributed to the changing of the group positions of the monomer. It is hypothesized that this structure provides benefits, including improved imprinted sites, accelerated mass transfer, and enhanced specific surface areas in comparison to the MIP based on phyopyroxle, phosthiopene, and their derivatives, which usually present a rapidly forming and intense structure. This MIP had a better group in the form of -COOH relative to the structures of phopyroxle, phosthiophene and their derivatives. The inclusion of this group likely enhanced the interactions with other groups in the FP molecular structure (e.g., -NH, -C=O, and -C-N). Ultimately, this endowed as-prepared sensor with higher sensitivity and selectivity.

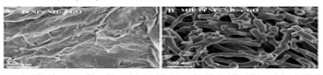

Figure 2. SEM images of Pt-NH$_2$-r-GO / GCE (A) and MIP-Pt NPs-NH$_2$-r-GO / GCE (B).

3.2 EISs of the modified electrodes

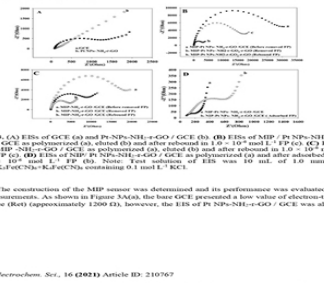

Figure 3. (A) EISs of GCE (a) and Pt-NPs-NH$_2$-r-GO / GCE (b). **(B)** EISs of MIP / Pt NPs-NH$_2$-r-GO / GCE (a, extracted (a), eluted (b) and after rebound in 1.0 × 10^{-9} mol L^{-1} FP (c). (C) EISs of MIP -NH$_2$-r-GO / GCE (a, polymerized (a), eluted (b) and after rebound in 1.0 × 10^{-9} mol L^{-1} FP (c). **(D)** EISs of NIP Pt NPs-NH$_2$-r-GO / GCE as polymerized (a) and after rebinded in 1.0 × 10^{-9} mol L^{-1} FP (b). Note: Test solution of EIS was 10 mL of 1.0 mmol L^{-1} $K_4Fe(CN)_6$+$K_3Fe(CN)_6$ containing 0.1 mol L^{-1} KCl.

The construction of the MIP sensor was determined and its performance was evaluated using EIS measurements. As shown in Figure 3A(a), the bare GCE presented a low value of electron-transfer resistance (Ret) (approximately 1200 Ω), however, the EIS of Pt NPs-NH$_2$-r-GO / GCE was almost a

straight line (Figure 3A(b)), indicating it enhanced the conductivity of the electrode. When MIP was polymerized on the above interface, the resulting electrode had a high Ret value (Figure 3B(a)); however, when the templates were eluted from MIP, the Ret decreased (Figure 3B(b)). This result indicated the recognition sites were formed in the polymer itself [19]. When MIP-Pt NPs-NH$_2$-r-GO / GCE was used to rebind FP (1 × 10^{-9} mol L^{-1}), its Ret value notably increased (Figure 3B(c)), indicating that the MIP had been successfully produced. For MIP-NH$_2$-r-GO / GCE (Figure 3C(a-c)), this change became smaller relative to that of MIP-Pt NPs-NH$_2$-r-GO / GCE. The reason for this change was due to the effect of Pt NPs, which enhanced the polymerization area and electron transfer capability. This then increased the recognition sites and signal amplification [20, 21]. As shown in Figure 3D (a-b) and regarding the NIP / Pt NPs- NH$_2$-r-GO / GCE, the change in Ret was approximately 400 Ω, indicating there were few, non-specific recognition sites that appeared on this interface.

3.3 Analytical performance of MIP sensor

To obtain the optimal response of the MIP sensor for FP, a series of experimental variables were next investigated, including mole ratio of FP to 6-IAA, electrochemical polymerization time, and adsorption time. Further detail regarding these variables is shown in SI (Figure S3). As shown in Figure 4A, the MIP-Pt NPs-NH$_2$-r-GO / GCE Ret increased with increasing FP concentration; moreover, in the range of 1.0 × 10^{-10} to 1.0 × 10^{-4} mol L^{-1} and 1.0 × 10^{-9} to 1.3×10^{-5} mol L^{-1}, it exhibited an evident linear response. The regression equations were Z'(Ω) = 3670 + 8587 C (μmol L^{-1}), r^2= 0.9930) and Z'(Ω) = 10082 + 1217 C (μmol L^{-1}), r^2= 0.9951) (Figure 4 B), respectively. The detection limit was 1.0× 10^{-10} mol L^{-1} (S/N= 3). Importantly, this sensor possessed a lower detection limit for compared to GC-MS / MS [4] and LC-MS / MS [5, 6, 22], the details were shown in Table 1.

Table 1. Comparison between the proposed MIP sensor with those reported in the literatures for FP detection

methods	Linear range (μmol L^{-1})	Limit of detection (μmol L^{-1})	Ref.
GC-MS/MS	0.001 – 0.025	0.0005	[4]
LC-MS/MS	0.0125 – 25	0.005	[5]
LC-MS/MS	0.0025 – 0.25	0.0025	[6]
LC-MS/MS	0.00025 – 0.025	0.00125	[22]
MIP sensor	0.001– 13	0.0001	This work

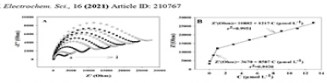

Figure 4. (A) EISs of MIP / Pt NPs-NH$_2$-r-GO / GCE in 1.0 mmol L^{-1} $K_4Fe(CN)_6$+$K_3Fe(CN)_6$ containing 0.1 mol L^{-1} KCl after binding in different FP concentrations of 0 (a) – 1.3 × 10^{-5} mol L^{-1} (j). (B) The calibration curve of MIP / Pt NPs-NH$_2$-r-GO / GCE for FP. Error bars represent SD (n= 3).

3.4 Stability reproducibility and selectivity, of the MIP sensor

To evaluate the performance of the as-prepared MIP sensor, selectivity, reproducibility, and stability were next assessed. For the selectivity experiments, bixafen and pyraclostrobin were selected as the interference agents. It had the expected sense when using the MIP sensor to measure 1.0 × 10^{-9} mol L^{-1} FP. However, it had a negligible response when using it to measure a 10-fold concentration of either bixafen or pyraclostrobin. The responses were primarily due to the presence of FP when using it to detect its coexistence (i.e., 1.0 × 10^{-9} mol L^{-1} FP + 1.0 × 10^{-7} mol L^{-1} bixafen and 1.0 × 10^{-9} mol L^{-1} FP +1.0 × 10^{-7} mol L^{-1} pyraclostrobin). Collectively, these results indicated that MIP plays a critical role in the selectivity of the electrochemical sensor (Figure S4).

The stability and repeatability of the MIP sensor were first explored using 1.0 × 10^{-9} mol L^{-1} of FP, resulting in a variation coefficient of 3.3% (n= 5). The Ret of the MIP sensor was maintained at 94.9% of its original value after 20 successive assays. The sensor was then maintained for 4 weeks at room temperature to explore its stability. Result indicated that the Ret of the MIP sensor was maintained at 94.0% (RSD= 4.1%, n= 5) of its original value. Five different electrodes were independently fabricated to evaluate the reproducibility by following the same procedure. A rest square deviation (RSD) of 5.8% was obtained for 1.0 × 10^{-9} FP, indicative of reliability of this fabrication method.

3.5 Detection of real samples

To test the practicability of the MIP sensor in real samples, recovery tests for FP in vegetables and fruits were next conducted. The samples were treated according to a previous report [22] and results are shown in Table 2. Recoveries were within the range of 96-112%. LC-MS / MS analysis further confirmed the recovery tests according to previously published work [22], consistent with the

MIP sensor data presented in Table 3, which indicated that the sensor was an excellent, practical option to detect FP in real samples.

Table 2. Recovery tests for FP in real samples by MIP sensor

Samples	Added (μmol L^{-1})	Found (μmol L^{-1})	Recovery (%)	RSD (%, n= 5)
Apple	0.00	0.00		
	0.50	0.48	96	4.1
	2.00	2.08	104	2.9
Cabbage	0.00	0.34		4.5
	0.50	0.90	112	4.9
	1.00	1.40	106	3.8

Table 3. LC-MS / MS method for FP in different samples

Samples	Added (μmol L^{-1})	Found (μmol L^{-1})	Recovery (%)	RSD (%, n= 5)
Apple	0.00	0.00		
	2.00	1.93	97.5	2.7
	5.00	4.95		6.4
Cabbage	0.50	0.95	114	6.6
	1.00	1.48	110	6.2

4. CONCLUSION

In this work, we used an easy method to prepare large amounts of Pt NPs with ultrasmall diameters (2-3 nm), which were then loaded onto NH$_2$-r-GO using HDPC as the structure-directing agent along with the interreaction between the amino group and Pt. The resulting product was then used to modify an electrode to provide a large surface area and good conductivity for MIP. 6-IAA was also used as a novel, functional monomer to construct an electrochemical sensor for FP. The final MIP had a three-dimensional, porous structure, which endowed the as-prepared sensor with excellent performance in the detection of FP. Collectively, these results indicated the utility of this type of sensor for detecting FP in real samples.

ELECTRONIC SUPPLEMENTARY INFORMATION

1. Optimization of assay conditions

We changed the mole ratio of template molecule to functional monomer from 1:1 to 1:6. The Ret value increased with this ratio decreased and a maximum value was obtained at 1:4, after, the Ret

value decreased (Fig. S3A). The effect of electrochemical polymerization time and MIP sensory response was recorded across a range of 8-20 cycles (Fig. S3B). As the polymerization time ranged from 8 to 16 cycles, the response increased, after which the response decreased. This observation was ascribed to the variety of recognition sites. The increase of polymerization time increased recognition sites, but also caused an increase of film thickness. As a result, recognition sites were buried in the MIP. Thus, 16 cycles was selected as the polymerization time.

To determine the effect of adsorption time for MIP sensor response, time was varied from 60 s to 420 s (Fig. S3C). Results indicated that the response leveled off as adsorption time reached 300 s and at a higher concentration level (e.g. 1.0×10^{-6} mol L^{-1}) of FP. Adsorption time was lengthened to 360 s at a low concentration (e.g. 5.0 × 10^{-9} mol L^{-1}). Thus, we chose 360 s as the optimal adsorption time, which ensured the MIP sensor had enough time to capture FP at a lower concentration.

2. Supplementary Figures

Fig. S1. SEM image of MIP-Pt NPs-NH$_2$-r-GO / GCE under low magnification.

Fig. S2. SEM image of MIP for florfenicol using 5-IAA as the functional monomer.

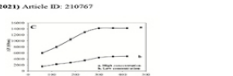

Fig. S3. Effect of different factors on the MIP sensor for 1.0 × 10^{-9} mol L^{-1} FP. All error bars represent SD (n= 3). (A) Ratio of template molecule to functional monomer. (B) Electrochemical polymerization time. (C) Adsorption time (e. 1.0 × 10^{-9} mol L^{-1}; b. 5.0 × 10^{-9} mol L^{-1} FP).

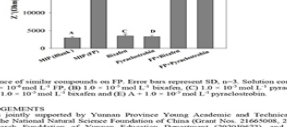

Fig. S4. Influence of similar compounds on FP. Error bars represent SD, n=3. Solution composition: (A) 1.0 × 10^{-9} mol L^{-1} FP, (B) 1.0 × 10^{-7} mol L^{-1} bixafen, (C) 1.0 × 10^{-7} mol L^{-1} pyraclostrobin, (D) A + 1.0 × 10^{-7} mol L^{-1} bixafen and (E) A + 1.0 × 10^{-7} mol L^{-1} pyraclostrobin.

ACKNOWLEDGEMENTS
This work was jointly supported by Yunnan Province Young Academic and Technical Leaders (2018HB005), the National Natural Science Foundation of China (Grant Nos. 21665008, 21277105), Scientific Research Fundation of Yunnan Education Department (2020J0672), and Scientific Research Fund Project of Honghe University (XJ16B04).

References

1. F. Dong, X. Chen, X. Liu, J. Xu, Y. Li, W. Shan and Y. Zheng, *J. Chromatogr. A.*, 1262 (2012) 98.
2. H. Liu, F. Liu, J. Yuan, F. Cui and J. Chen, *Sci. Total Environ.*, 769 (2021) 144519.
3. A. Crépet, T. M. Luong, J. Baines, P. E. Boon, J. Ennis, M. Kennedy, I. Massarelli, D. Miller, S. Nako, R. Renzo, H. J. Voos and P. Verger, *Food Control*, 121 (2021) 107583.
4. Y. Shen, Z. Li, Q. Ma, C. Wang, X. Chen, Q. Miao and C. Hao, *J. Agric. Food Chem.*, 64 (2016) 5.
5. A. Abad-Somovilla, E. Caballos-Alcantarilla, J. V. Mercader, C. Agulló, A. Abad-Somovilla and F. A. Esteve-Turrillas, *Anal. Bioanal. Chem.*, 407 (2015) 4207.
6. F. You, C. Qiao, J. Liao, L. Guo, T. Pang, R. Peng, J. Li, C. Wang, R. Wang and H. Nie, *J. Chromatogr. B*, 1152 (2020) 122261.
7. W. Wang, X. Wang, N. Cheng, Y. Luo, Y. Lin, W. Xu and D. Du, *TrAC Anal. Chem.*, 132 (2020) 116031.
8. F. Zhao, J. Wu, Y. Ying, Y. She, J. Wang and J. Ping, *TrAC Anal. Chem.*, 106 (2018) 62.
9. X. Hou, L. Xu, T. Zhen and W. Wu, *Food Anal Sci Technol.*, 105 (2020) 76.
10. L. Bezerra, E. Conte-Ramos, R. Segato, J. G. Pacheco, H. P. A. Nouws, M. N. D. S. Cordeiro and C. Delerue-Matos, *Biosens. Bioelectron.*, 172 (2021) 112719.
11. M. Mahmoodpour, M. Torbati, M.-M. Mousavi, M. de la Guardia and J. Ezzati Nazhad Dolatabadi, *TrAC Anal. Chem.*, 129 (2020) 115943.
12. F. Zouaoui, S. Bouroumina-Bacha, M. Bouroumina, N. Jaffrezic-Renault, N. Zine and A. Errachid, *TrAC Anal. Chem.*, 130 (2020) 115982.
13. A. Fan, G. Yang, H. Yang and F. Zhao, *Master Today Chemistry*, 25 (2020) 101448.
14. L. Guo, H. Zhang, C. Zhang, L. Qu and L. Xu, *Talanta*, 210 (2020) 120631.
15. L. Guo, H. Zhang, C. Zhang, L. Qu and L. Xu, *Talanta*, 210 (2020) 120631.
16. K. Parate, C. Kannakaran and J. C. Claussen, *Sensor Actuator. B Chem.*, 287 (2019) 165.
17. Q. Guo, F. Hu, N. Yang, J. Yang, S. Yang, X. Chen, F. Wu and S. D. Minteer, *Microchem. J.*, 158 (2020) 105254.
18. G. Yang and F. Zhao, *J. Mater Chem. C*, 2 (2014) 10201.
19. Chun Yang, X. F. Ji, W. Q. Cao, J. L. Wang, Q. Zhang, T. L. Zhong and Y. Wang, *Sensor. Actuator. B Chem.*, 282 (2019) 818.
20. F. Zouaoui, S. Bouroumina-Bacha, M. Bouroumina, I. Abeza-Nemeir, H. Ben Halima, J. Gallardo-Moreno, M. L. Ruiz-Bravo, N. Jaffrezic-Renault, S. Bouchta, N. Jaffrezic-Renault, N. Zine and A. Errachid, *Sensors Actuators B. Chem.*, 309 (2020) 127753.
21. B. Khadro, C. Sanglar, A. Bouhoume, A. Errachid and N. Jaffrezic-Renault, *Procedia Engineering*, 5 (2010) 371.
22. S. Li, X. Liu, Y. Zhu, F. Dong, J. Xu, M. Li and Y. Zheng, *J. Chromatogr. A.*, 1358 (2014) 46

© 2021 The Authors. Published by ESG (www.electrochemsci.org). This article is an open access article distributed under the terms and conditions of the Creative Commons Attribution license (http://creativecommons.org/licenses/by/4.0/).

大学英语四级考试
成绩报告单

CET®

姓　　名：石玲

学　　校：南昌大学

院（系）：理学院

准考证号：[redacted]

身份证号：

考试时间：2006 年 6 月

总分：425

听力 (20%)	阅读 (40%)	综合 (25%)	写作 (15%)
151	160	52	62

成绩单编号：[redacted]

教育部高等教育司

委托发布单位：全国大学英语四、六级考试委员会

考委会网址：www.cet.edu.cn

5、 学术能力证明材料

1 篇代表性论文

中国科学院武汉科技查新咨询检索中心

检 索 报 告

（报告编号：2025-WJ-0909-2）

委托单位：红河学院					
委 托 人：石玲					
检索要求：2020 年发表第一作者论文“A novel electrochemical immunosensor for aflatoxin B1 based on Au nanoparticles-poly 4-aminobenzoic acid supported graphene”被 SCIE 收录与相关期刊 2020 年升级版分区情况					
检 索 结 果					
数据库	论文收录(篇)				
SCIENCE CITATION INDEX-EXPANDED	1				
数据库	2020 年大类分区情况				
中国科学院文献情报中心期刊分区表-升级版	分区	1 区	2 区	3 区	4 区
	篇数	0	1	0	0
*相关期刊分区信息见附件。					
声明	委托人接受本证明，视为已对本证明所列论文逐篇核对，确认无误，若有不实，由委托人承担全部责任。				
检索人	万杰	审核人	[signature]		

中国科学院武汉科技查新咨询检索中心

（公章）

2025-04-09

联系人：万杰 联系电话：027-87197719

邮箱：chaxin@mail.whlib.ac.cn

主页：www.whlib.ac.cn

地址：武汉市武昌区小洪山西 25 号

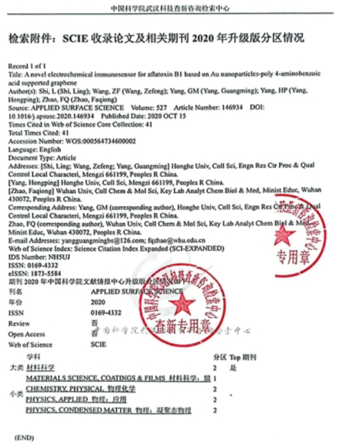

中国科学院武汉科技查新咨询检索中心

检索附件：SCIE 收录论文及相关期刊 2020 年升级版分区情况

Record 1 of 1

Title: A novel electrochemical immunosensor for aflatoxin B1 based on Au nanoparticles-poly 4-aminobenzoic acid supported graphene

Author(s): Shi, L (Shi, Ling); Wang, ZF (Wang, Zefeng); Yang, GM (Yang, Guangming); Yang, HP (Yang, Hongping); Zhao, FQ (Zhao, Faqiong)

Source: APPLIED SURFACE SCIENCE Volume: 527 Article Number: 146934 DOI: 10.1016/j.apsusc.2020.146934 Published Date: 2020 OCT 15

Times Cited in Web of Science Core Collection: 41

Total Times Cited: 41

Accession Number: WOS:000564734600002

Language: English

Document Type: Article

Addresses: [Shi, Ling; Wang, Zefeng; Yang, Guangming] Honghe Univ, Coll Sci, Engn Res Ctr Proc & Qual Control Local Characteri, Mengzi 661199, Peoples R China.

[Yang, Hongping] Honghe Univ, Coll Sci, Mengzi 661199, Peoples R China.

[Zhao, Faqiong] Wuhan Univ, Coll Chem & Mol Sci, Key Lab Analyt Chem Biol & Med, Minist Educ, Wuhan 430072, Peoples R China.

Corresponding Address: Yang, GM (corresponding author), Honghe Univ, Coll Sci, Engn Res Ctr Proc & Qual Control Local Characteri, Mengzi 661199, Peoples R China.

Zhao, FQ (corresponding author), Wuhan Univ, Coll Chem & Mol Sci, Key Lab Analyt Chem Biol & Med, Minist Educ, Wuhan 430072, Peoples R China.

E-mail Addresses: yangguangmingbs@126.com; fqzhao@whu.edu.cn

Web of Science Index: Science Citation Index Expanded (SCI-EXPANDED)

IDS Number: NH5UJ

ISSN: 0169-4332

eISSN: 1873-5584

期刊 2020 年中国科学院文献情报中心升级版分区情况 [illegible]

刊名	APPLIED SURFACE SCIENCE
年份	2020
ISSN	0169-4332
Review	否
Open Access	否
Web of Science	SCIE

	学科	分区	Top 期刊
大类	材料科学	2	是
小类	MATERIALS SCIENCE, COATINGS & FILMS 材料科学：膜	1	
	CHEMISTRY, PHYSICAL 物理化学	2	
	PHYSICS, APPLIED 物理：应用	2	
	PHYSICS, CONDENSED MATTER 物理：凝聚态物理	2	

(END)

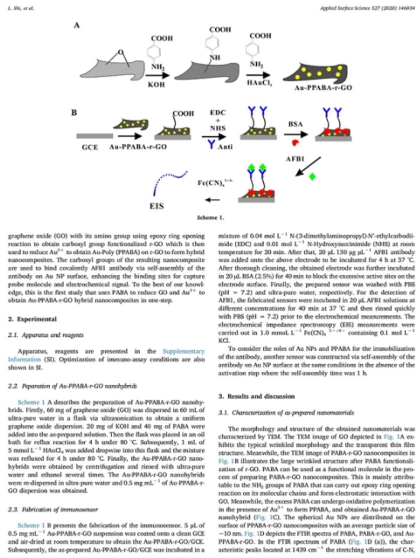

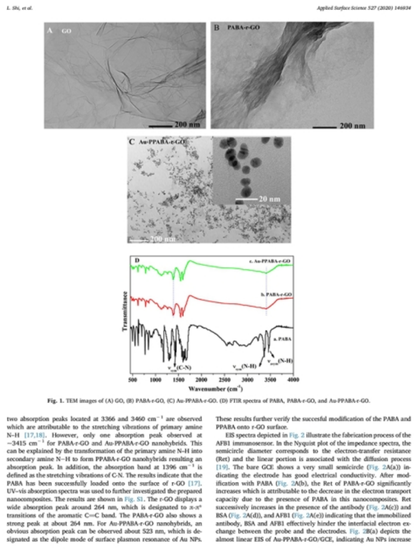

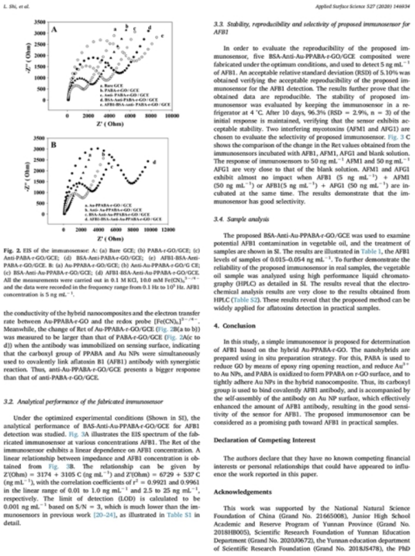

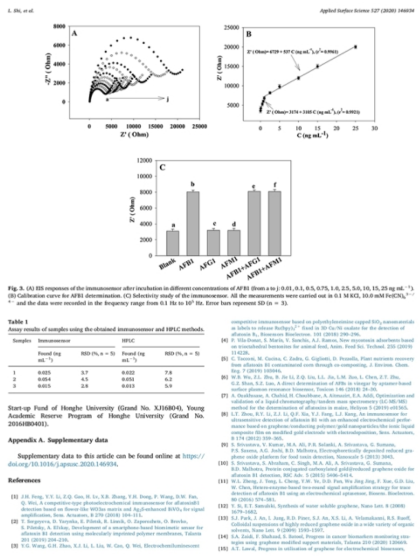

1 项其他代表性成果

中国科学院武汉科技查新咨询检索中心

证 明

（报告编号：2025-WJ-0909-8）

委托单位：红河学院
委托人：石玲

经检索，期刊《MICROCHIMICA ACTA》(ISSN: 0026-3672)是 SCIENCE CITATION INDEX-EXPANDED 收录的源刊。

MICROCHIMICA ACTA

期刊 2025 年中国科学院文献情报中心升级版分区信息如下：

刊名	MICROCHIMICA ACTA
年份	2025
ISSN / EISSN	0026-3672 / 1436-5073
Review	否
OA Journal Index（OAJ）	否
Open Access	否
Web of Science	SCIE

学科	分区	Top 期刊
大类 化学	2	否
小类 CHEMISTRY, ANALYTICAL 分析化学	2	-

特此证明！

中国科学院武汉科技查新咨询检索中心
检索人：万杰
2025-04-09
联系人：万 杰 联系电话：027-87197719
邮箱：chaxin@mail.whlib.ac.cn
主页：www.whlib.ac.cn
地址：武汉市武昌区小洪山西 25 号

Microchimica Acta (2025) 192:307
https://doi.org/10.1007/s00604-025-07157-2

RESEARCH

A novel ionic-liquid-supported polythieno[3,2-b]thiophene coating for headspace solid-phase microextraction of phenolic compounds from environmental water via gas chromatography-mass spectrometry

Ling Shi[1] · Anping Li[1] · Yuying Xu[1,3] · Hongping Yang[2] · Guangming Yang[1]

Received: 22 January 2025 / Accepted: 6 April 2025
© The Author(s), under exclusive licence to Springer-Verlag GmbH Austria, part of Springer Nature 2025

Abstract
A novel thieno[3,2-b]thiophene (TT) was utilized for the first time to electrochemically fabricate an ionic liquid (IL)-supported polythieno[3,2-b]thiophene (PTT) coating. This innovative coating serves as a new headspace solid-phase microextraction (HS-SPME) material for the extraction of five phenolic compounds, which were subsequently determined via gas chromatography-mass spectrometry (GC–MS). The coating was characterized using Fourier-transform infrared spectroscopy, scanning electron microscopy, and energy-dispersive X-ray spectroscopy. Experimental results confirmed that the ILs were successfully embedded within the polymer matrix, resulting in a well-defined three-dimensional mesoporous architecture. This unique architecture not only exhibited high thermal stability but also maintained a consistent extraction performance when used for the solid-phase microextraction of phenolic compounds. To optimize the extraction and detection performance, various experimental parameters were investigated, including the coating type, pH, salt concentration, extraction time, extraction temperature, stirring rate, desorption time, and temperature. Under the optimal conditions identified, the method exhibited low limits of detection ranging from 0.001 to 0.007 μg mL^{-1} and wide linearity in the concentration range 0.030 to 10.000 μg mL^{-1}. Noteworthily, the proposed method was successfully applied to the determination of five phenols in actual water samples, achieving satisfactory recoveries between 90.5% and 110.5%.

Keywords Gas chromatography-mass spectrometry · Headspace solid phase microextraction · Ionic liquid · Phenolic compounds · Polythieno[3,2-b]thiophene

Introduction

Sample preparation is a crucial step in analytical methods, particularly when dealing with extremely low analyte concentrations in complex matrices. Conventional extraction methods often require large amounts of hazardous solvents and exhibit low sensitivity for the detection of trace levels of compounds.

Solid-phase microextraction (SPME) addresses these challenges as a solvent-free, cost-efficient, and versatile approach that consolidates the sampling, isolation, and analytical processes into a single workflow [1]. Importantly, SPME can be easily coupled with advanced analytical techniques such as gas chromatography (GC), high-performance ...

Yuying Xu
2052000755@qq.com
Guangming Yang
yangguangmingbs@126.com
1 Yunnan Province International Joint Laboratory of Green Food (China-Vietnam), School of Chemistry and Resources Engineering, Honghe University, Mengzi 661199, People's Republic of China
2 Honghe University, Mengzi 661199, People's Republic of China

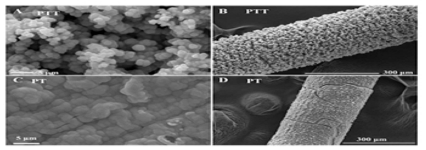

Fig. 1 SEM images of (A and B) PTT and (C and D) PT coatings

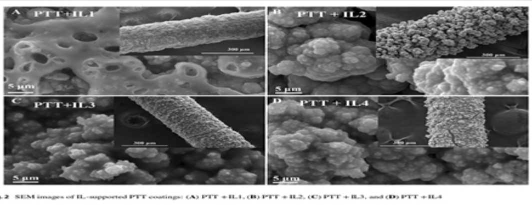

Fig. 2 SEM images of IL-supported PTT coatings: (A) PTT + IL1, (B) PTT + IL2, (C) PTT + IL3, and (D) PTT + IL4

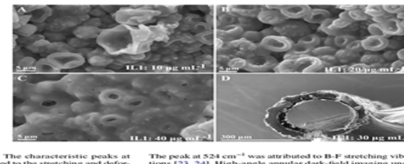

Fig. 3 SEM images of PTT + IL1 coatings with different concentrations of IL1

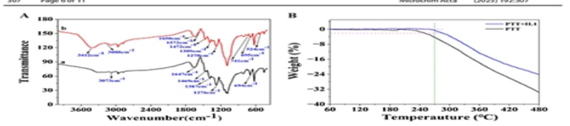

Fig. 4 A The FT-IR spectra of (a) PTT and (b) PTT + IL1. B Thermogravimetry (TG) analysis of PTT and PTT + IL1 coating

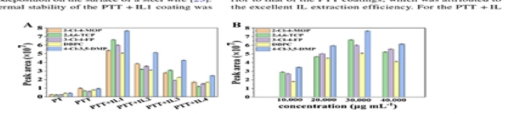

Fig. 5 A Comparison of the extraction efficiency of the PT, PTT, PTT + IL1, PTT + IL2, PTT + IL3, and PTT + IL4 coating for the five phenols. B The influence of the concentration of IL1 on extraction efficiency of PTT + IL coating for the five phenols

1 项其他代表性成果

中国科学院武汉科技查新咨询检索中心

检 索 报 告

(报告编号：2025-WJ-0909-5)

委托单位：红河学院

委 托 人：石玲

检索要求：2022 年发表第一作者论文“Preparation of 3D Nanoflower-like ZnO/graphene Oxide decorated with Au@AuPt Bimetallic Nanoparticles for Electrochemical Determination of Doxorubicin Hydrochloride”被 SCIE 收录与相关期刊 2022 年升级版分区情况

检 索 结 果

数据库	论文收录(篇)			
SCIENCE CITATION INDEX-EXPANDED	1			
数据库	2022 年大类分区情况			
中国科学院文献情报中心期刊分区表-升级版	分区	1 区	2 区	3 区	4 区
	篇数	0	0	0	1

*相关期刊分区信息见附件。

声明	委托人接受本证明，视为已对本证明所列论文逐篇核对，确认无误，若有不实，由委托人承担全部责任。		
检索人	万杰	审核人	[illegible]

中国科学院武汉科技查新咨询检索中心

(公章)

2025-04-09

联系人：万杰 联系电话：027-87197719

邮箱：chaxin@mail.whlib.ac.cn

主页：www.whlib.ac.cn

地址：武汉市武昌区小洪山西 25 号

检索附件：SCIE 收录论文及相关期刊 2022 年升级版分区情况

Record 1 of 1

Title: Preparation of 3D Nanoflower-like ZnO/graphene Oxide decorated with Au@AuPt Bimetallic Nanoparticles for Electrochemical Determination of Doxorubicin Hydrochloride

Author(s): Shi, L (Shi, Ling); Wang, ZF (Wang, Zefeng); Bai, LE (Bai, Lae); Yang, GM (Yang, Guangming)

Source: INTERNATIONAL JOURNAL OF ELECTROCHEMICAL SCIENCE Volume: 17 Issue: 1 Article Number: 220144 DOI: 10.20964/2022.1.45 Published Date: 2022 JAN

Times Cited in Web of Science Core Collection: 10

Total Times Cited: 10

Accession Number: WOS:000743605300007

Language: English

Document Type: Article

Addresses: [Shi, Ling; Wang, Zefeng; Bai, Lae; Yang, Guangming] Honghe Univ, Coll Sci, Engn Res Ctr Proc & Qual Control Local Characteri, Mengzi 661199, Peoples R China.

[Wang, Zefeng] Shanghai Univ Tradit Chinese Med, Innovat Res Inst Tradit Chinese Med IRI, Shanghai 201203, Peoples R China.

Corresponding Address: Wang, ZF; Yang, GM (corresponding author), Honghe Univ, Coll Sci, Engn Res Ctr Proc & Qual Control Local Characteri, Mengzi 661199, Peoples R China.

Wang, ZF (corresponding author), Shanghai Univ Tradit Chinese Med, Innovat Res Inst Tradit Chinese Med IRI, Shanghai 201203, Peoples R China.

E-mail Addresses: wangzefeng841006@163.com; yangguangmingbs@126.com

Web of Science Index: Science Citation Index Expanded (SCI-EXPANDED)

IDS Number: YI1GV

ISSN: 1452-3981

期刊 2022 年中国科学院文献情报中心升级版分区情况如下：

刊名	International Journal of Electrochemical Science
年份	2022
ISSN	1452-3981
Review	否
Open Access	否
Web of Science	SCIE

学科	分区	Top 期刊
大类 化学	4	否
小类 ELECTROCHEMISTRY 电化学	4	-

(END)

Int. J. Electrochem. Sci., 17 **(2022)** Article Number: 220144, doi: 10.20964/2022.1.45

International Journal of ELECTROCHEMICAL SCIENCE

www.electrochemsci.org

Preparation of 3D Nanoflower-like ZnO/graphene Oxide decorated with Au@AuPt Bimetallic Nanoparticles for Electrochemical Determination of Doxorubicin Hydrochloride

Ling Shi[1], *Zefeng Wang*[1,2,*], *Lae Bai*[1], *Guangming Yang*[1,*]

[1] Engineering Research Center for Processing and Quality Control of Local Characteristic Food and Consumer Goods of High Education in Yunnan Province, College of Science, Honghe University, Mengzi 661199, PR China

[2] Innovation Research Institute of Traditional Chinese Medicine (IRI), Shanghai University of Traditional Chinese Medicine, Shanghai 201203, China

*E-mail: wangzefeng841006@163.com, yangguangmingbs@126.com

Received: 14 October 2021 / *Accepted:* 23 November 2021 / *Published:* 6 December 2021

A novel 3D nanoflower-like ZnO-graphene oxidation (3D ZnO-GO) nanocomposites were proposed for the first time by simple aqueous hydrothermal method and sonochemical approach. Then the Au@AuPt NPs were decorated onto 3D ZnO-GO nanocomposites to obtain a novel Au@AuPt/3D ZnO-GO nanohybrids. The obtained nanohybrids were characterized by scanning electron microscopy, transmission electron microscopy, and X-ray diffraction. The Au@AuPt/3D ZnO-GO nanohybrids were used to fabricate electrochemical sensor for detection of doxorubicin hydrochloride. The proposed sensor showed excellent electrocatalytic activity toward electrochemical oxidation doxorubicin hydrochloride. The electrochemical ocidation reaction of doxorubicin hydrochloride on modified electrode surface was a surface-controlled process, and the charge transfer coefficient (α) and electron transfer number (n) were 0.81 and 2, respectively. The sensor had a wide linear range from 0.65 μM to 369.45 μM, with the limit of detection was 0.013 μM. Furthermore, the proposed electrochemical sensor can be applied successfully to selective determination of doxorubicin hydrochloride in urine sample.

Keywords: Graphene oxidation; Au nanoparticles; Pt nanoparticles; Zinc oxide; doxorubicin hydrochloride; electrochemical sensor

1. INTRODUCTION

Doxorubicin hydrochloride was an important anticancer drug, which had been widely used for the treatment of breast cancer, lymphoma and bladder cancer in clinical treatment [1]. However, the

clinical application of doxorubicin hydrochloride was limited because of some toxic side effects including cardiotoxicity, alopecia, myelosuppression, hypoalbuminemia [2, 3]. Thus, it was necessary to monitor the doxorubicin hydrochloride concentrations in patient's serum or urine to avoid adverse effects and ensure the effectiveness of the treatment and patient safety [4, 5]. Therefore, it was urgently necessary to develop fast, simple, and selective methods for detection of doxorubicin hydrochloride. Electrochemical detection technique had received a dramatic growth in recent years due to wide range application and low cost [6, 7]. As well-known, a great diversity of nanomaterials had been demonstrated exhibiting wonderful properties and can enhance electrochemical performance of proposed sensor.

Recently, Zinc oxide (ZnO) had been thought to be a prominent multifunctional material for electrochemical sensor applications due to its good biocompatibility, nontoxicity, and high chemical stability. The variety of structures of ZnO nanomaterials had been reported, 1D nanorods, needles, and wires, 2D nanoplate, nanosheet, and nanopellets, 3D flower, snowflakes, and coniferous urchin-like. However, pure ZnO usually showed rapid recombination of charge carriers which would limit its application. Graphene oxidation nanosheets exhibited unique performance, such as, excellent chemical stability, high conductivity, and high specific surface area, and would provide an exciting new array of ideas and applications. Based on the above considerations, many researchers had prepared the nanocomposites of reduced graphene oxide with ZnO [8, 9]. Nevertheless, the report about 3D flower-like ZnO-graphene oxidation was relatively few. Meantime, the application of novel Au@AuPt bimetallic nanoparticle decorated flower-like ZnO-graphene oxidation (Au@AuPt/3D ZnO-GO) nanohybrids as high-performance electrocatalysts for constructing a doxorubicin hydrochloride electrochemical sensor had rarely been explored.

In this work, a novel 3D flower-like ZnO was prepared by a simple aqueous hydrothermal method, and then 3D flower-like ZnO-GO nanocomposites were obtained for the first time through a sonochemical approach. Then the Au@AuPt NPs were decorated onto 3D ZnO-GO nanocomposites to obtain a novel nanohybrid. The obtained nanohybrid was used to construct electrochemical senor for doxorubicin hydrochloride.

2. EXPERIMENTAL

2.1. Chemicals

Graphene oxidation was obtained from Jiangsu XFNANO Technology Co., Ltd. Zinc nitrate hexahydrate [$Zn(NO_3)_2 \cdot 6H_2O$], hexamethylenetetramine ($C_6H_{12}N_4$), trisodium citrate dihydrate ($HOC(COONa)(CH_2COONa)_2 \cdot 2H_2O$), anhydrous ethanol, phosphoric acid, glacial acetic acid, boric acid were obtained from Shanghai Chemical Reagent Co. Ltd. (Shanghai, China). Tetrachloroauric (III) acid ($HAuCl_4$), hexachloroplatinic (IV) acid (H_2PtCl_6), doxorubicin hydrochloride were purchased from Shanghai Eybridge Chemical Technology Co., Ltd. A certain amount of doxorubicin hydrochloride was dissolved in Ultra-pure water with ultrasonication for 30 min, and stored in the dark at 4 ◦C. The Britton-Robinson (B-R) buffer solutions (0.04 M in each of acetic, phosphoric and boric

acids) adjust to the desired pH with additions of 0.2 M sodium hydroxide were used as a supporting electrolyte.

2.2. Synthesis of 3D flower-like ZnO and ZnO-GO nanocoposites

0.7437 g $Zn(NO_3)_2 \cdot 6H_2O$ was dissolved in 250 mL ultra-pure water in a round-bottom flask. 0.14 g $C_6H_{12}N_4$ was dissolved in 100 mL ultra-pure water and then added into the above solution under magnetic stirring. 0.0735 g trisodium citrate dehydrate was dissolved in 50 mL ultra-pure water and continued adding to the above solution. The obtained mixed solutions were kept at 95 °C with constant stirring for 2 h. The resultant 3D flower-like ZnO was collected by centrifugation and washed with ultra-pure water and anhydrous ethanol three times. The obtained nanomaterials were marked as ZnO-2.

In order to prepare 3D flower-like ZnO-GO nanocoposites, 10.0 mg GO was dispersed in 10 mL ultra-pure water. The mixture solutions was ultrasonicated for 1 h. Then as-prepared 30 mg 3D ZnO was added into the GO suspension. The obtained solution was subjected to ultrasound (200 W) for 2 h at 50 °C, leading to a light grey solution. The obtained solution was stored at 4 °C for later use.

2.3. Synthesis of Au nanoseeds

Au nanoseeds were prepared according to a modified Frens' method [10]. 1.30 mL 19.302 mM $HAuCl_4$ solution and 48.8 mL ultra-pure water were mixed in three-necked round bottom flask. Then the obtained solution was heated to a boil. Then 0.368 mL 340 mM trisodium citrate solutions were added. The obtained solutions were vigorous stirred and refluxed for 10 min. Finally, the obtained wine red dispersion was stored at 4 °C after cooling.

2.4. Synthesis of Au@AuPt NPs and Au@AuPt/3D ZnO-GO nanohybrids

In a typical method, 2 mL of Au nanoseeds, 1.5 mL of H_2PtCl_4 (1.00 mM) and $HAuCl_4$ (nH_2PtCl_4: $nHAuCl_4$ = 2:1) were mixed in three-necked round bottom flask. The resultant solution was kept at 4 °C under vigorous stirring for 5 min, followed by addition of 0.65 mL $NaBH_4$ (10.00 mM). The mixture was stirred for approximately 30 min. The resulting products were collected by centrifugation and washed with ultra-pure water. Finally, the obtained Au@AuPt NPs were dispersed in 30 mL ultra-pure water. For the syntheses of Au@AuPt/3D ZnO-GO nanohybrids, 30 mL Au@AuPt NPs and 10 mL 3D flower-like ZnO-GO were mixed, then the mixture solutions were ultrasonicated (200 W) for 3 h. the resulting homogeneous dispersion solutions were collected.

2.5. Characterization of the synthesized nano-materials

The morphologies of the as-prepared 3D ZnO and 3D ZnO-GO nanocomposites were observed on a high resolution field emission scanning electron microscopy (SU8010, Hitachi). And the

morphologies of Au@AuPt/3D ZnO-GO nanohybrids were further studied by transmission electron microscope (JEOL 2010, operating at 200 KV). Crystalline properties of the prepared nano-materials were examined using X'Pert³ powder diffractometer (PANAlytical Company).

2.6. Electrochemical measurements

Before the surface coating, the GC electrode (GCE, 3 mm in diameter) was polished carefully with 1.0, 0.3, and 0.05 μm alumina powder and rinsed with ultra-pure water, followed by sonication in ethanol and ultra-pure water successively. For electrochemical experiments, 7 μL of prepared nanocomposites were dropped on the surface of the GCE and dried in air. The fabricated sensor was used as the working electrode for all electrochemical studies. The electrochemical experiments were performed with a CHI 660E electrochemical analyzer (CH Instruments, Chenhua Co., Shanghai, China). A conventional three-electr ode cell was used, including a Ag/AgCl (saturated KCl) electrode as reference electrode, a platinum wire as counter electrode, and modified GC as working electrode. Electrochemical impedance spectroscopy (EIS) was performed in 1.0 mM $[Fe(CN)_6]^{3-/4-}$ containing 0.1 M KCl as supporting electrolyte within the frequency range of 0.1—10^5 Hz. The cyclic voltammetry (CV) were carried out in pH=6.0 B-R buffer solution containing 30 μM doxorubicin hydrochloride. The differential pulse voltammetry (DPV) measurments were recorded in the range of 0.2-0.8 V with the applied parameters as follows: amplitude was 0.05 V, pulse width was 0.05 s.

2.7. Analysis of real samples

We used human urine as real samples to determine the doxorubicin hydrochloride content by standard addition method. A certain amount of each real sample was diluted with pH=6.0 B-R buffer solution, spiked with doxorubicin hydrochlorid and then tested to measure doxorubicin hydrochlorid by DPV.

3. RESULT AND DISCUSSION

3.1. Synthesis and characterization of prepared nanomaterials

Flower-like ZnO nanocomposites were prepared under solvothermal condition. $Zn(NO_3)_2 \cdot 6H_2O$ was used as reactive material, $C_6H_{12}N_4$ was used as uniform precipitant which provided hydroxide ions (OH^-), and trisodium citrate dehydrate used as surface modification agent. In this hydrothermal process, the preparing of flower-like ZnO was endured two-step nucleation growth process. Firstly, $C_6H_{12}N_4$ can provide OH^- according to the equation (1) and (2), the $Zn(NO_3)_2 \cdot 6H_2O$ provided Zn^{2+}. The $Zn(OH)_2$ can be obtained when $Zn(NO_3)_2 \cdot 6H_2O$ was mixed with $C_6H_{12}N_4$. Because exist of excess hydroxide ions in the solution, the freshly prepared $Zn(OH)_2$ readily got converted into $[Zn(OH)_4]^{2-}$ (Equ (3)). Then the ZnO crystal nucleus were formed by the dehydration reaction of $[Zn(OH)_4]^{2-}$ (Equ (4)).

$$(CH_2)_6N_4 + 6H_2O \rightarrow 6HCHO + 4NH_3 \quad \text{Equ (1)}$$

$$NH_3 + H_2O \rightarrow NH_4^+ + OH^- \quad \text{Equ (2)}$$

$$Zn^{2+} + 2OH^- \rightarrow NH_4^+ + [Zn(OH)_4]^{2+} \quad \text{Equ (3)}$$

$$[Zn(OH)_4]^{2+} \rightarrow ZnO + H_2O + 2OH^- \quad \text{Equ (4)}$$

At this stage, a large amount of ZnO crystal nucleus would be produced as the reaction proceeds. The newly formed ZnO nucleus were constantly incorporated into the initial nucleus, and then nanoclusters with certain orientations were formed [11, 12]. The trisodium citrate could reduce surface energy of nanoclusters and regulate nucleation and growth of secondary structures. Then the ZnO nanoclusters grew into a spherical structure and the side length of the ZnO nanosheets increased significantly as the reaction time increased [13]. It was noted that ZnO nanosheets crossed each other and resulting formed a porous network structure. The morphological of ZnO was characterized by scanning electron microscopy (SEM) images. The reaction time was optimized varied from 1 h to 4 h in order to obtain better flower-like structure ZnO. The results were shown in Figure 1 A-H, the obtained ZnO revealed a spherical morphology with diameter ranging from 2 to 3 μm when the reaction time was 1.0 h. And the part of the ZnO surfaces had not formed porous network structure. When the reaction time was increased to 2.0 h, the sheet-like ZnO plates were getting thinner and thinner, the crossover was becoming more obvious resulting a large number of 3D pores structure were formed onto the surface of ZnO structure. Figure 1D revealed the ZnO consisted of numerous nanoflowers, most of nanoflowers were integrated rather than just aggregated with each other. When the reaction time was extended to 3 h, the nanosheets that form the pores structure became rougen and thicken. Finally, at the reaction time of 4 h, the characteristic flower-like structure was disintegrating, and the pores structure was fewer (Figure 1G and 1H). The results proved that the well-defined 3D flower-like ZnO can be obtained when the reaction time was 2 h.

After ultrasound reaction in GO suspension, the surface of 3D flower-like ZnO were coated by thin layers of GO film, the results were shown in Figure 2A. The size of 3D ZnO-GO nanoflowers was about 2.2 μm. It is worth noting that the ZnO still have a 3D flower-like after ultrasound reaction in ZnO-GO nanoflowers. There was no obvious structural changes and collapses, indicating great structural stability. The composite possessed a stable structure due to the introduction of GO nanosheets, which utilizes bend to maintain thermodynamic stability of nanohybrids. Remarkably, the 3D ZnO-GO nanoflowers still possessed a number of pores among petals, which would offer more specific surface area and help not only to load a large number of nanoparticles, but also to increase the contact area between the electrode material and small molecules. It would benefit to accelerate electron transfer during the electrochemical reaction.

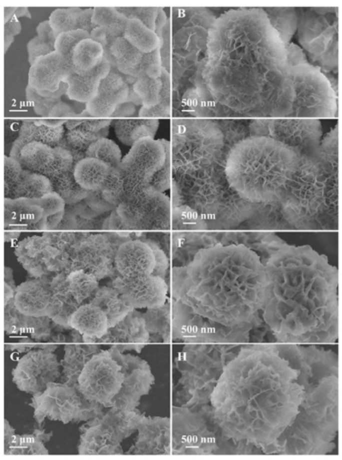

Figure 1. SEM images of 3D ZnO-1 (A and B), 3D ZnO-2 (C and D), 3D ZnO-3 (E and F), and 3D ZnO-4 (G and H), which were obtained with the reaction time of 1 h, 2 h, 3 h, and 4 h, respectively.